Liquid Crystals
Publication details, including instructions for authors and subscription information:
http://www.informaworld.com/smpp/title~content=t713926090

Electrooptic response of smectic O and smectic O

P. E. Cladis[a]; Helmut R. Brand[b]
[a] AT&T Bell Laboratories, Murray Hill, New Jersey, U.S.A. [b] FB 7, Physik, Universität Essen, Essen, Germany

To cite this Article Cladis, P. E. and Brand, Helmut R.(1993) 'Electrooptic response of smectic O and smectic O', Liquid Crystals, 14: 5, 1327 — 1349
To link to this Article: DOI: 10.1080/02678299308026446
URL: http://dx.doi.org/10.1080/02678299308026446

LIQUID CRYSTALS, 1993, VOL. 14, NO. 5, 1327–1349

Electrooptic response of smectic O and smectic O*

by P. E. CLADIS*† and HELMUT R. BRAND‡
† AT&T Bell Laboratories, Murray Hill, New Jersey 07974, U.S.A.
‡ FB 7, Physik, Universität Essen, D 4300 Essen 1, Germany

We present the results of our investigations on the electrooptic properties of the smectic O and O* phases of m7tac (1-methylheptyl terephthalylidene-bis-4-aminocinnamate). At low voltages, we observed striking electrochromic effects and, in O* at high voltages, a field induced phase transition. Freely suspended thick films of m7tac in the O and O* phases are weakly biaxial. A framework is proposed to account for our observations.

1. Motivation: chevron smectic phases

In 1983, Levelut *et al.* [1] reported the existence of a new smectic liquid crystal phase in m7tac (1-methylheptyl terephthalylidene-bis-4-aminocinnamate, see figure 1). They called this phase smectic O. While the molecular length of m7tac is about 46 Å, the observed layer spacing in the smectic O* (or smectic O in the racemate) phase is only 31 Å [2]. Levelut *et al.* thus proposed a structure for smectic O* (O) that was similar to smectic C* (C, see figure 2) with the long axis of m7tac inclined at an angle $\theta \sim \cos^{-1}(31\text{ Å}/46\text{ Å}) \sim 48°$ to the layer normal. This is an unusually large angle for tilted smectic phase.

Because their proposed structure seemed, at first sight, incompatible with their observation of $S = 1/2$ line defects [3], our interest was stimulated in the electrooptic response of smectic O* in chiral m7tac as well as that of smectic O in the m7tac racemate.

In 1983, Patrick Keller sent us samples of m7tac^{++}, m7tac^{--} and m7tac racemate, where the plus and minus signs refer to the chirality of the asymmetric carbons (shown with a star (*) in figure 1) at each end of m7tac. For m7tac^{++} both asymmetric carbons are right handed, for m7tax^{--} both are left handed. The m7tac racemate is a mixture of m7tac^{+-} (50 per cent), m7tac^{++} (25 per cent) and m7tac^{--} (25 per cent). In [4] Keller discusses the synthesis and the sensitivity of the occurrence of smectic O to alkyl chain length.

Another remarkable feature of m7tac is the enhanced thermal stability of the racemate compared to chiral m7tac. In 1983, we found that the chiral compounds transform to smectic Q* (see note under [5]) at 129·12°C (heat of transition, 0·45 cal g^{-1}) and smectic Q* transforms to the isotropic liquid at 132·9°C (0·12 cal g^{-1}) making a total energy difference between smectic O* and the isotropic liquid of 0·57 cal g^{-1}. In contrast, the racemate releases about twice the heat at the transition to the isotropic liquid, i.e. 1·31 cal g^{-1}, at a much higher temperature, i.e. 156°C! The origin of the remarkable thermal stability of the racemate compared to chiral m7tac is significant and requires understanding. In this paper, we propose and discuss a possible

* Author for correspondence.

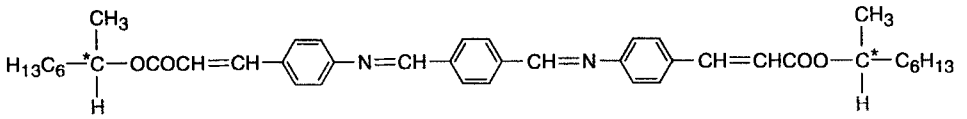

Figure 1. Molecular structure of m7tac (molecular weight ~649). The asymmetric carbons are marked with stars (*). The molecule is highly symmetric.

model involving microscopic segregation of $m7tac^{++}$ and $m7tac^{--}$ from $m7tac^{+-}$ isomers.

Our arguments are based on observations made in 1983 on the m7tac compounds [6], as well as recent results on the time dependence of the electrooptic response of smectics O and O*. In 1983–1986, we found that the electrooptic response of the m7tac compounds differed qualitatively from classical tilted smectic phases in both chiral and non-chiral compounds [7].

In particular, while the low frequency response of O* was complicated, the high frequency (1 kHz) response showed colour changes with increasing voltage up to $\sim 10\,V\,\mu m^{-1}$. While we will most simply refer to colour changes observed in O* in a high frequency field as an electrochromic effect, we stress that crossed polarizers are required to observe it. Thus, in contrast to microscopic mechanisms invoked to explain the, perhaps, more familiar electrochromic effect observable without crossed polarizers, the two macroscopic mechanisms we consider to account for this electrochromic effect in smectic O* are: (i) a change in helical pitch, i.e. helix unwinding, and (ii) field enhanced in-plane biaxiality. Above $\sim 10\,V\,\mu m^{-1}$, we observed an electric field induced transition reminiscent of helix unwinding at the cholesteric→nematic field induced transition. However, there are important differences between our observations on the field induced transition in O* and the cholesteric→nematic transition.

First, the observed field induced textures were consistent with negative in-plane dielectric anisotropy. Second, the optic axes between crossed polarizers in the field induced state were ~45° to the optic axes of the state just before the transition. Third, while the field induced state took seconds to nucleate and grow, when the applied electric field was removed, the zero voltage state returned faster than could be captured on video-tape ($\leqslant 0{\cdot}1$ s). The implication here is that, unlike the cholesteric→nematic field induced transition, the high field state induced in O* is more ordered than the zero field smectic O*: near threshold, order takes time to grow while, far from threshold, disorder takes place as a relaxation process [8]. This is consistent with the observation that front propagation is the growth mechanism for the high field state of smectic O* while, far from threshold, the zero field state returned as a rapid relaxation process.

We also observed colour changes as a function of temperature and applied voltage in the smectic O phase of m7tac racemate. In addition, we observed a weak linear (i.e. the change in contrast depended on the sign of the applied electric field) electrooptic effect at low frequencies (less than 1 Hz) and low voltages (less than $2\,V\,\mu m^{-1}$) that depended on the orientation of the optic axis relative to the axes of crossed polarizers and the temperature. Finally, we found that freely suspended thick films of smectic O were optically weakly biaxial and that freely suspended thick films of both smectic O and smectic O* showed stable $S=1$ defects. But, the free energy of two $S=1/2$ defects (topologically equivalent to a single $S=1$ defect) is half that of a single $S=1$. So, this observation is at odds with the Levelut *et al.* observation [1] of $S=1/2$ defects that are excluded by their proposed structure for smectic O.

Interestingly, in a somewhat earlier paper, Hardouin *et al* [9] noted similarities in the X-ray pattern of smectic O* in m7tac and of a phase they called $S_?$ in a chlorine substituted cyano compound DB_8Cl (octylphenyl 2-chloro-4-(*p*-cyanobenzoyloxy-benzoate)) that was observed to have bilayer smectic A and C phases. DB_8Cl transformed from a bilayer smectic C phase to a lower temperature $S_?$. They remarked that this new phase might correspond to "molecular or bimolecular anisotropy changes".

More recently, Galerne and Liébert [10] proposed a chevron structure for smectic O* (and O) in m7tac. In their model (see figure 3(*a*)), deduced from optical studies of smectics O and O*, the molecular tilt alternates between $\pm\theta$ on neighbouring layers of the chevron structure. Galerne and Liébert point out that this structure made smectic O* "optically equivalent to a biaxial smectic A phase" [10]. This statement is somewhat ambiguous because a biaxial smectic A allows $S=1/2$ defects, while the chevron structure does not [3]. However, $S=\pm 1/2$ disclinations combined with a screw dislocation in the layers is topologically possible for the chevron structure [11, 12].

While the possibility of a chevron structure for liquid crystals was raised at least as far back as 1977 [13], X-ray evidence for a chevron structure was first reported in a main chain liquid crystal polymer in 1988 [14]. The sensitivity of the chevron structure to the length of the alkyl spacer links in the polymer back-bone was also noted [14]: the chevron structure occurred in the odd-numbered homologues and a smectic A structure in the even-numbered homologues.

Once more our interest was renewed in smectic O. Our initial interest was stimulated by the recent discovery by Leube and Finkelmann [15] of a biaxial smectic A phase (called smectic C_M, where the M stands for Macmillan [16], the first to discuss such a phase, see figure 2) in a side on side chain liquid crystalline polymer. We noted [3] that $S=1/2$ line defects are only compatible with smectic C_M symmetry and incompatible for a classical tilted smectic structure (see, for example figure 2). Here [3], we also point out that, by symmetry, the chevron structure is antiferroelectric independent of molecular chirality (see figure 3(*a*)) and introduced a novel smectic structure that we called smectic C_P, where P stands for the spontaneous polarization, that, by symmetry, could exist independent of molecular chirality (see figure 2).

At the 1992 German Liquid Crystal Meeting (21. Freiburger Arbeitstagung Flüssigkristalle), Heppke *et al.* [17], realizing that the chevron structure of a chiral compound (but not a non-chiral one) such as $m7tac^{++}$ or $m7tac^{--}$ is locally antiferroelectric, reported the miscibility of the smectic O* phase of m7tac and the antiferroelectric smectic phase discovered by Chandani *et al.* [18]. Heppke *et al.* also noted the sensitivity of the occurrence of smectic O phases to alkyl chain length and reported a ferroelectric *P-E* hysteresis loop for chiral m7tac, not an antiferroelectric one [17].

Although several different physical techniques were used to characterize the antiferroelectric phases, Chandani *et al.* [18] were the first to observe the characteristic double hysteresis loop. They called the antiferroelectric phase smectic C_{A^*} and also proposed a chevron structure to account for antiferroelectricity in the chiral compound. In their compounds the tilt angle ($\sim 25°$) is not as large as in m7tac. It was also determined that smectic C_{A^*} occurred at a lower temperature than smectic C* and was not miscible with either smectic C* or smectic I*. Indeed, detailed investigations of several compounds exhibiting smectic C_{A^*} phases have been made by many researchers [18, 19]. In the racemate model of Takanishi *et al.* [20], the left- and right-handed

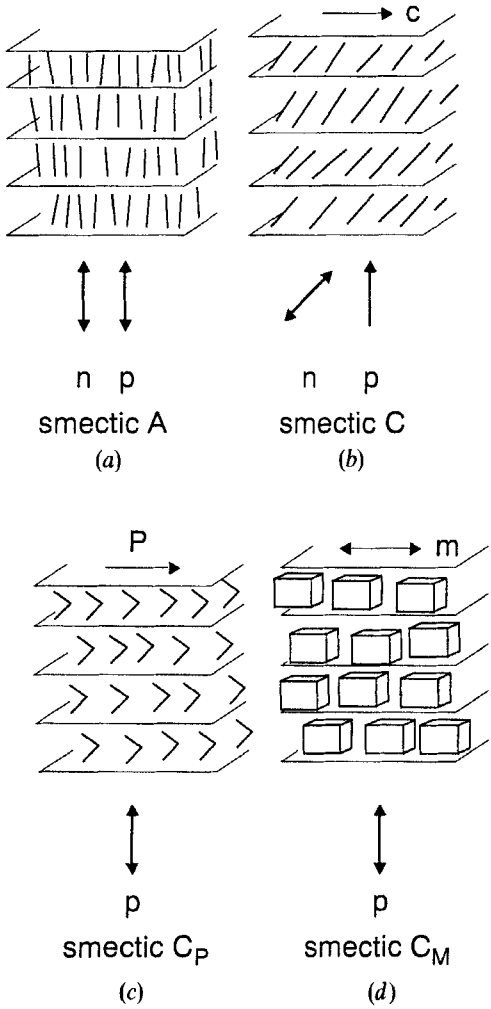

Figure 2. Structure of various smectic phases (from [3]): **p** is the layer normal, **n** is the director, **c** and **m** are the in-plane director in smectic C and smectic C_M, respectively, and **P** is the polarization. The smectic phases depicted have the following symmetries: (*a*) smectic A: $D_{\infty h}$, (*b*) smectic C: C_{2h}, (*c*) smectic C_P: C_{2v}, and (*d*) smectic C_M: D_{2h}.

enantiomers are assumed mixed within a layer and the overall structure is again a chevron structure.

Most recently, optical observations of $S = \pm 1/2$ disclinations in combination with a screw disclination (a dispiration with no discontinuity of the in-plane optic axis) in smectic C_{A^*} that disappeared on heating into smectic C* were also reported [11, 12]. These authors [11, 12] finally conclude that "the antiferroelectric structure is optically equivalent to cholesteric liquid crystals". While the dislocation associated with a dispiration is one in the helix pitch in C_{A^*} [11], they have also been observed in the racemate, i.e., C_A [12].

In view of these exciting new developments, it is appropriate to review our old results [6] on the electrooptic effects in smectic O and smectic O*. Because of our recent

symmetry argument for the chevron structure [3], we pay particular attention to the electrooptic response of smectic O in the racemate of m7tac.

2. Chevron symmetry and polarization states

We take the z direction to be normal to the smectic layers, the x direction to be parallel to the layers in the plane of figure 3 and the x–z plane to be the symmetry plane. Figure 3 (*a*) shows a chevron structure in the x–z plane. We consider first the non-chiral case. In any layer, the director tilt is uniform relative to the z axis, the layer normal. On neighbouring layers, the tilt is equal in magnitude but opposite in sign. Considering the layers two at a time, we note that the x direction is a two-fold axis, the axis of highest symmetry, and the x–y plane is a vertical mirror plane. The appropriate classification is C_{2v} [21] with a polarization vector $\mathbf{P} \| \mathbf{x}$. The sign of the polarization **P** depends on which pair of layers is chosen and alternates from layer to layer, giving rise to antiferroelectricity in a non-chiral smectic chevron structure when the layer–layer interactions are the same for all layers (see figure 3 (*a*)). If the layer interactions are different, then the magnitude of **P** will depend on which pair of layers is chosen, giving rise to ferrielectricity in a non-chiral chevron smectic structure (see figure 3 *b*)), that also has C_{2v} symmetry.

Indeed, if the interlayer interactions could be continuously varied with temperature, say, or concentration, we can easily imagine a material where the macroscopic polarization, **P**, varied continuously from antiferroelectric to ferroelectric (see, for example figure 2) [3] in the chevron structure for non-chiral compounds.

Interlayer interactions of a highly symmetric compound (such as m7tac, see figure 1) in a chevron structure (such as figure 3 (*a*)) are indistinguishable from layer to layer making antiferroelectricity a likely property of these materials. For less symmetric molecules [18], a distinction between the two ends of the molecules raises the

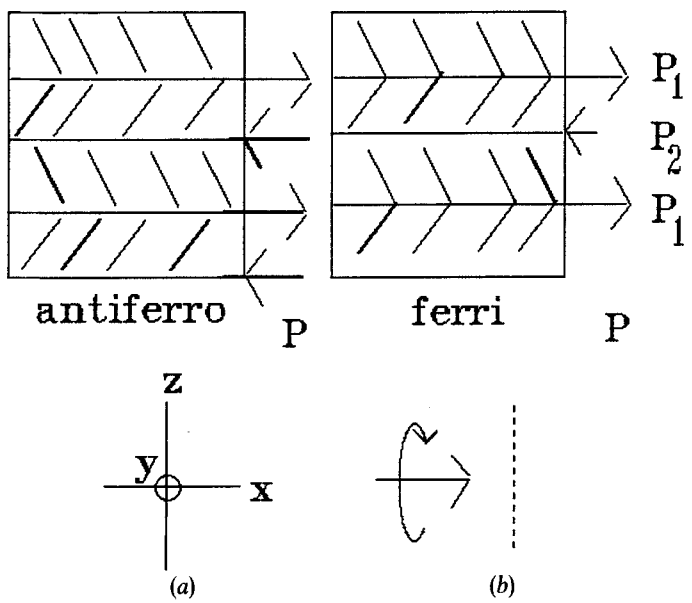

Figure 3. (*a*) The chevron structure for smectic O. We point out here that this structure can be antiferroelectric in non-chiral systems. (*b*) When layer–layer interactions alternate from layer to layer, a ferrielectric structure results.

possibility in a racemate for ferrielectric states (see figure 3(*b*)) rather than antiferroelectric ones. Current models do not consider the possibility of polarization states for a racemate in a chevron structure.

We now consider the more subtle case of chiral molecules in a chevron smectic structure. If there is molecular chirality, then there are no mirror planes and the highest symmetry is C_2 [22]. As in the non-chiral case, the x direction is a two-fold axis locally with P_1 for one pair of layers and P_2 opposite in sign to P_1 for the next pair of layers. If the magnitude of P_1 is not the same as that of P_2, then **x** is the only two-fold axis for this structure. **y** is an additional two-fold axis (the same as for classical tilted smectics [22]), *if and only if* P_1 *is equal in magnitude to* P_2.

In the models put forward by Chandani *et al.* [18] and Galerne and Liébert [10] for the chiral chevron structure, the sign of P_y alternates from layer to layer (being positive for one sign of the tilt angle and negative for the other) and **y** is the only two-fold axis they consider. Symmetry arguments show that this is inconsistent with the chevron structure for which we argue there is always a two-fold axis in the x direction. The picture emerging from our analysis of the symmetry associated with the chevron structure is that the plane of the antiferroelectric polarization vector in the chevron structure is at some angle to the x–z plane of figure 3 depending on the strengths of the two components of **P**.

In summary, for chiral compounds in the chevron structure, **P** is locally in the chevron plane for ferroelectric and ferrielectric states and at some angle, $(\pi/2-\beta)$, to the chevron plane for antiferroelectric states. In contrast, for ferroelectric states of the tilted smectic phases of chiral molecules, **P** is perpendicular to the plane of tilt (i.e. the plane spanned by the director and the layer normal [22]). While it may be difficult to detect a 90° or β in-plane rotation of **P** between smectic C*, say, and a chiral chevron state, this information would provide direct support for the existence of chevron type smectic structures.

As is well known, in fluid tilted smectics formed by chiral molecules, there is a helix structure with an axis perpendicular to the layers. Therefore, **P** is helical and globally $\langle \mathbf{P} \rangle \equiv 0$ making the state helielectric not ferroelectric [7]. The arguments that have been presented for the chiral states are local symmetry arguments, i.e. arguments valid on length scales much smaller than the helical pitch.

The sign of the dielectric anisotropy can also play a significant role. In that case, more electrooptic states are available when non-linear electric field effects become important in smectic O and O* at large magnitudes and high frequencies of the applied electric field.

Given the symmetry of m7tac (see figure 1), we can imagine a monolayer smectic C_P^* structure such as shown in figure 4(*a*) where in one layer $P_y = 0$, because **y** is not a two-fold axis. There is a net polarization, $P_x \neq 0$, as shown in the figure, associated with a single smectic layer for the same symmetry argument given for smectic C_P (see figure 2). For a fluid smectic phase, there will also be a helix structure as observed in chiral smectic phases with fluid in-plane order. When the two chains are tilted in the same direction (see figure 4(*b*)), then the y axis is a two-fold axis and $P_y \neq 0$, while $P_x = 0$ locally. For a chiral system, the transition from figure 4(*a*) (C_2) to figure 4(*b*) (C_2) is accompanied by a 90° rotation of P. Such a transformation could be effected by a single *cis–trans* conformational change. The energy for such a single *cis–trans* conformational change about a single carbon–carbon bond can range from 3 to 10 kcal mol^{-1} [23] depending on the other substituents. Figure 4(*a*) shows the local structure of a fluid C_P^* on a scale much smaller than the pitch of the helix structure in which it is embedded. In

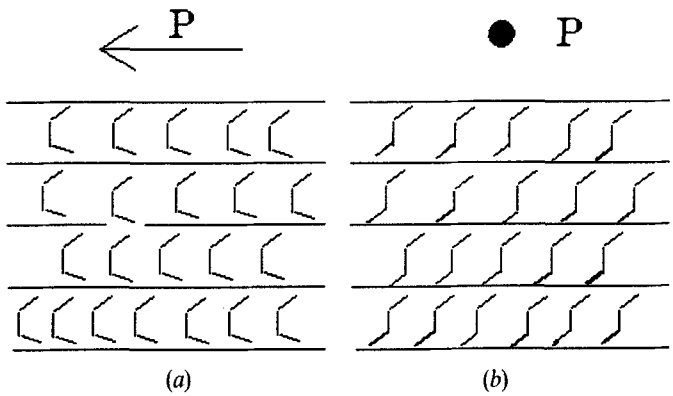

Figure 4. (*a*) Local structure of a possible C_P^*. Given the in-plane fluidity of C_P^*, globally a helical structure is expected to make C_P^* helielectric. The plane of the figure is the x–z plane. (*b*) A microscopic model for the high field state of a chiral system. The solid circle indicates a spontaneous polarization perpendicular to the plane of the figure.

the simplest structure, the helix axis is perpendicular to the layers. While the polarization states supported by the chevron structure may range from ferroelectric to antiferroelectric, the P–E loop for C_P^* is expected to be ferroelectric or ferrielectric, depending on interlayer interactions. While a ferroelectric P–E loop for chiral m7tac has been reported [17], more information on its frequency dependence is required before ferrielectricity and antiferroelectricity can be excluded in chiral m7tac.

In one model [18] for C_{A^*}, the unit that rotates is a chevron composed of a pair of layers giving rise to two helices out of phase by π. For the racemate, C_A, left-handed enantiomers form chevron pairs and so do right-handed enantiomers [20]. According to this picture, left- and right-handed species mix on a microscopic scale within each layer [20], so that, globally, there is still C_{2v} symmetry and the possibility of antiferroelectricity.

The conclusion is that, despite structural similarities, there are many possibilities for the electrooptic states of smectic O* and smectic O. While miscibility studies [17] show that both smectic O* and smectic C_{A^*} have the same local symmetry (C_2) [22], polarization states can range continuously from ferroelectric to antiferroelectric [3] and, indeed, there is evidence that they do [17]. While the low field state of O* is not miscible [18] with I* (nor C*), the question arises—is the apparently more ordered high field state miscible with a tilted smectic phase? Finally, while the chiral species of O* and C_{A^*} are miscible [17], it would be useful to check the miscibility of their racemates.

3. Observations

3.1. *Optical observations*

Textures of chiral and racemic m7tac in freely suspended thick ($\sim \mu$m) films were studied by polarizing microscopy. We summarize here these observations recorded on videotape from 1983 to 1986 when it was still believed that the structure of these phases was similar to classical fluid tilted smectics with a very large tilt angle [1].

At that time, we were surprised by the weakness in biaxiality (optical bisectrix was normal to the film) in freely suspended thick films of both chiral and racemic m7tac.

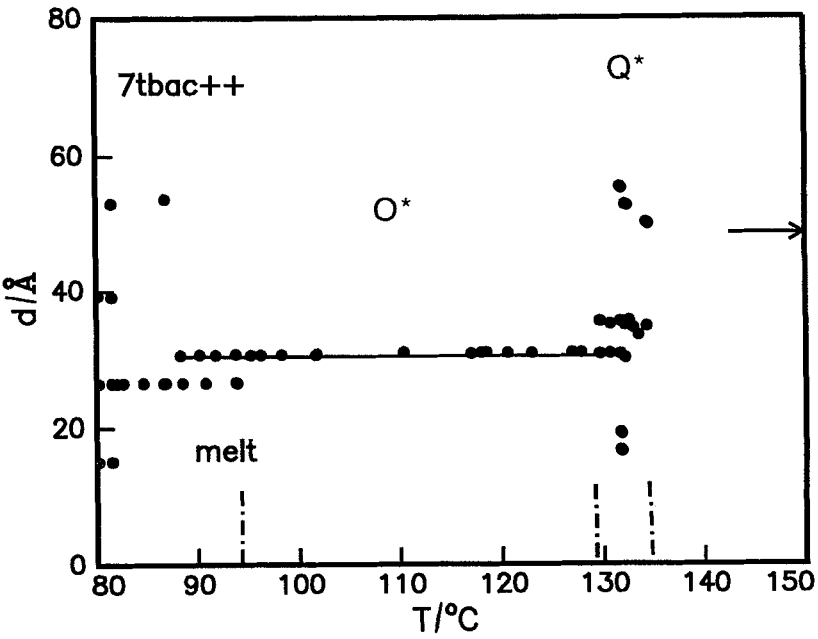

(*a*)

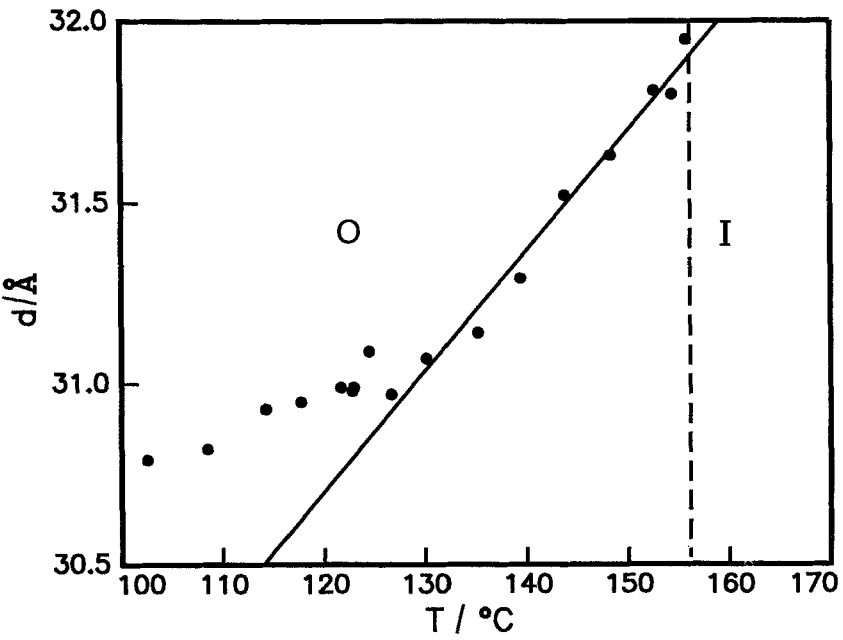

(*b*)

Figure 5. Measurements in (*a*) and (*b*) have the same accuracy; only the plotting scales are different in the two figures. (*a*) Layer spacing of m7tac^{++} as a function of temperature; the arrow on the right shows the fully extended length of the molecule: ~46 Å. The layer spacing in smectic O* is independent of temperature within ±0·2 Å. The tilt in O* is, thus, ~48°. (*b*) Layer spacing of m7tac racemate as a function of temperature. Above about 120°C the layer spacing increases linearly with temperature.

While a similar thick film in a smectic C phase with half the tilt angle of smectic O is relatively bright, the m7tac racemate film looked nearly homeotropic.

A typical thick film in the smectic C* phase is optically active and uniaxial because of its helix structure. In contrast, films of chiral m7tac were birefringent and failed a simple test for optical activity. The birefringence of the chiral film suggested that we had drawn films much thinner than the pitch.

In the new light shed by chevron models [10, 18], we will consider another possibility: the two asymmetric carbons of chiral m7tac compensate the optical activity of each other because the all-*trans* configuration for this particular homologue of mntac in one smectic layer is more similar to the conformation sketched in figure 4 (*a*) (a monolayer chevron) than it is to the molecular conformation sketched for a classical tilted layer (see, for example, figure 4 (*b*)). Indeed, we will argue that this possibility best fits the unusual opto-electronic effect observed in chiral m7tac in the dielectric regime, i.e. high frequencies.

Films of m7tac racemate were much easier to draw than were those of $m7tac^{--}$. Both species showed in-plane fluctuations similar to those observed in fluid smectic phases, in-plane textures that could be interpreted as walls, and, long-lived $S=1$ disclinations. While a chevron lamellar structure is proposed for both the chiral-antiferroelectric materials and their racemates [10, 18, 20], we consider here the possibility that the molecular arrangements in a layer are qualitatively different in the two species. While not excluding other possibilities, we argue that this possibility is the simplest one to account for our observations in m7tac.

3.2. *X-ray measurements*

X-ray measurements of the layer spacing of m7tac as a function of temperature were made in 1984. Figure 5 (*a*) shows the data for $m7tac^{++}$. The data for $m7tac^{--}$ are similar. The layer spacing in smectic O* is independent of temperature and $30{\cdot}6 \pm 0{\cdot}2$ Å. In contrast, while the layer spacing of the racemate is weakly temperature dependent in the temperature range where smectic O* is stable, it has a linear growth of 0·033 Å K^{-1} in the range where only the racemate is stable (see figure 5 (*b*)). DSC measurements did not detect a phase transition in the racemate associated with this change in temperature dependence in the racemate. These small variations in the layer spacing suggest that the origin of thermochromic effects observed in m7tac is linked either to the temperature dependence of the in-plane biaxiality or to a change in the helix pitch.

The arrow on the right of figure 5 (*a*) shows the fully elongated length of a single molecule of m7tac. The absence of diffraction peaks in the smectic O phase corresponding to a layer spacing comparable to or larger than a single molecular length does not obviously support a bilayer structure. However, given that the strongest X-ray scattering is expected from the aromatic cores where the electron density is largest, the observed diffraction could be compatible with a bilayer structure with the same electron density within a layer (associated with the aromatic cores) and aliphatic chains (more transparent to X-rays) with different orientations in neighbouring layers.

In conclusion, the simplicity of the smectic O/O* diffraction pattern and the shortness of the only spacing observed are consistent with a uniformly tilted smectic as originally suggested [1]. For it to be consistent with a bilayer chevron structure, the electron rich aromatic cores in both layers comprising a bilayer structure must be similarly oriented, with the distinguishing feature of each layer arising from the disposition of the aliphatic chains that are relatively transparent to X-rays.

3.3. *Electrooptic effect in smectic O**

Figure 6 shows a 12 μm thick sample of m7tac^{--} in a polarizing microscope. The polarizer and analyser are crossed and parallel to the sides of each frame. The smectic layers are curved with the layer normals in the plane of each photomicrograph and perpendicular to the applied AC electric field ($f = 1$ kHz). Dramatic colour changes, with a potential for applications, are observed as a function of applied field that are not conveyed by these polaroid snapshots taken from the video monitor screen as a video tape of the experiment was playing. The sequence in figure 6 was taken with increasing applied field and is shown here to demonstrate the effect qualitatively. At 100 V, a new state, where the optics axis (roughly speaking the black parts in each frame) is now rotated by 45° relative to the state before this field induced transition, nucleates and spreads rapidly in the plane of some layers. Growth of this new state proceeds more slowly perpendicular to the layers. In the final state, the region that was bright at zero voltage is now black and, conversely, the regions that were black at zero voltage are now bright. When the field is turned off, the zero voltage state snaps back within one video frame (i.e. the relaxation to the zero field state (see figure 7) takes place in less than 0·1 s).

We use space–time plots to quantify this electric field induced transition at constant voltage and temperature. Figure 8 shows four views in the polarizing microscope of a

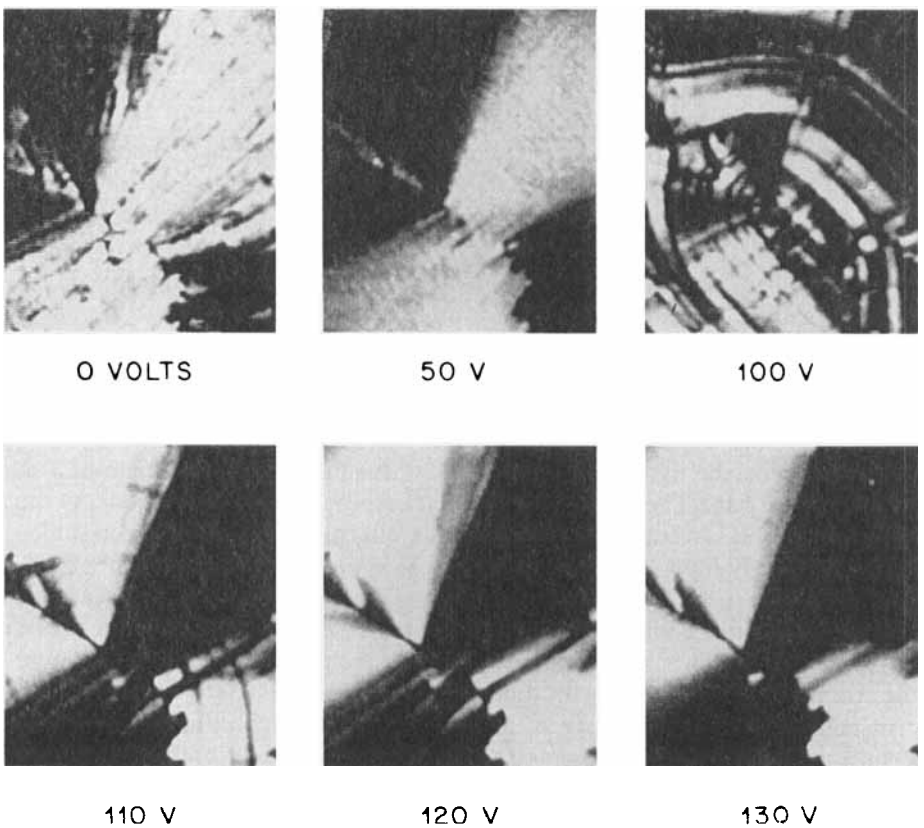

Figure 6. Photomicrographs of the field induced transition in m7tac^{--} as a function of voltage. The frequency of the applied field is 1 kHz.

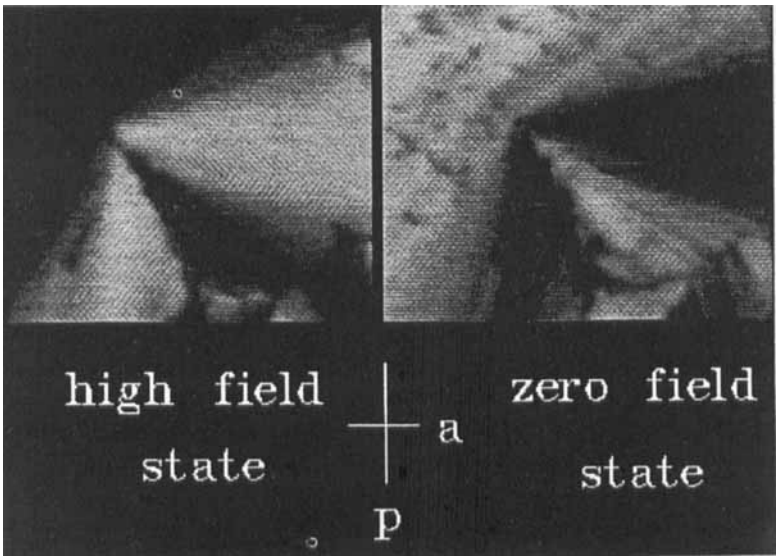

Figure 7. The high field state on the left transforms to the zero field state shown on the right in less than 0·1 s after the field is turned off.

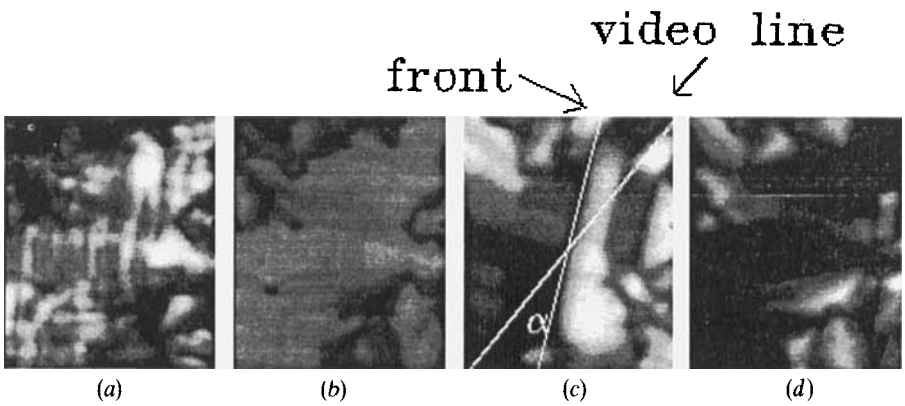

Figure 8. Description of the generation of space-time plots. (*a*) $V=0$. (*b*) Just after a field $V=10\,\mathrm{V}/\mu\mathrm{m}^{-1}$ has been applied. (*c*) High field state (black) invading low field state. The video line that is collected every 0·22 s and the actual front are shown as white lines and include an angle of $\alpha=27°$. (*d*) High field state.

small part of a polycrystalline preparation of m7tac^{--}. The temperature is 113°C and the sample is 13 μm thick. In figure 8 (*a*) the field is off. Figure 8 (*b*) shows the change in contrast observed just after a 1 kHz square wave of about 10 V $\mu\mathrm{m}^{-1}$ has been applied; these experiments are clearly in the regime where the dielectric contribution of the electric field energy dominates. After a delay, τ, figure 8 (*c*) shows a black contrast invading a brighter region from the left. A white line has been placed at the front of the advancing black region. The second white line, at an angle $\alpha=27°$ to this line, shows the video line (about 55 μm in length) that is grabbed every 0·22 s then replotted in sequence to make a space–time record of the observations. Figure 8 (*d*) shows the final high field state.

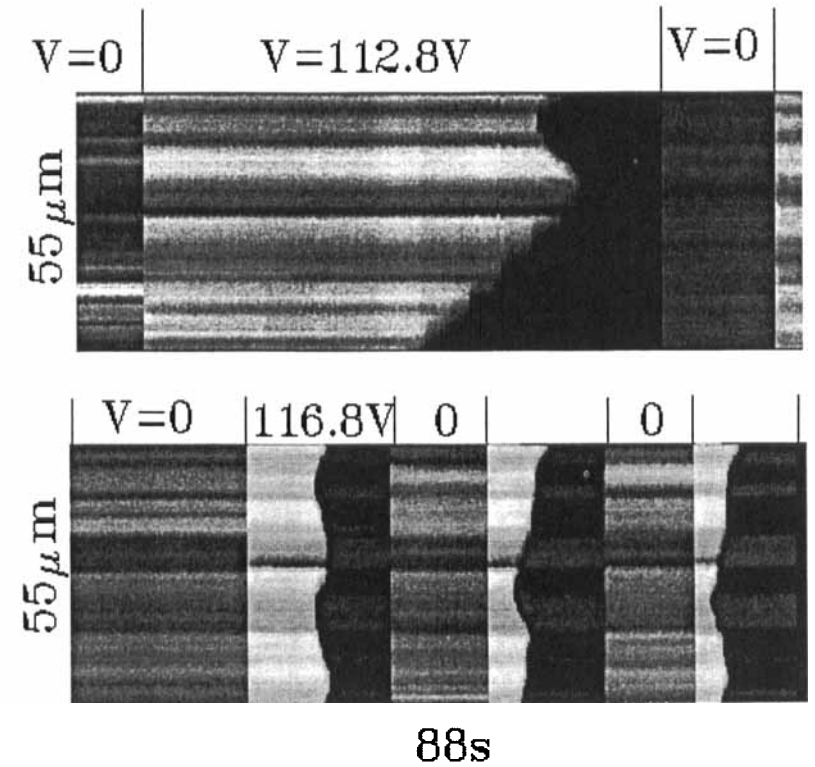

Figure 9. Space–time plots of the field induced transition at $T = 113°C$.

Figure 9 shows space–time plots for two voltages. In this figure, the vertical axis is space ($\sim 55\ \mu m$) and the horizontal axis is time. The complete time for the sequences shown in figure 9 is 400 video lines or 88 s. We look first at the space–time plot for the applied field of 112·8 V (see top of figure 9).

At zero applied field, the field of view is dark. When 112·8 V is applied, the field of view immediately lightens due to colour changes caused by changing the in-plane birefringence, but there is no rotation of the optic axis (see figure 6). There is a lag of duration τ before a second change is first observed. The speed at which the black region invades the white region is given by the slope of the line separating the two regions. While structure is observed on this line, the average speed, v, at which the black contrast moves across the video line is approximately constant. Front propagation is, thus, an important mechanism for the growth of the high field state into the low field state. We also note, even excluding the delay time, the time for this transition to take place is in the order of tens of seconds. In contrast, when the field is turned off after the black region has completely invaded the sample, the original $V = 0$ state is restored within 0·2 s, the time resolution of this plot.

The second space–time plot shown at the bottom of figure 9 is taken at a higher voltage. Here the effect of continually cycling the sample into the high field state can be appreciated: the delay decreases significantly and the average speed increases.

Figure 10 (*a*) shows $\ln(\tau)$ (τ is the delay time for the first occurrence of the high field state in the field of view) and figure 10 (*b*) shows $\ln(v)$ (v is the average front speed) as a function of the applied voltage. From these data, the activation potential Φ is

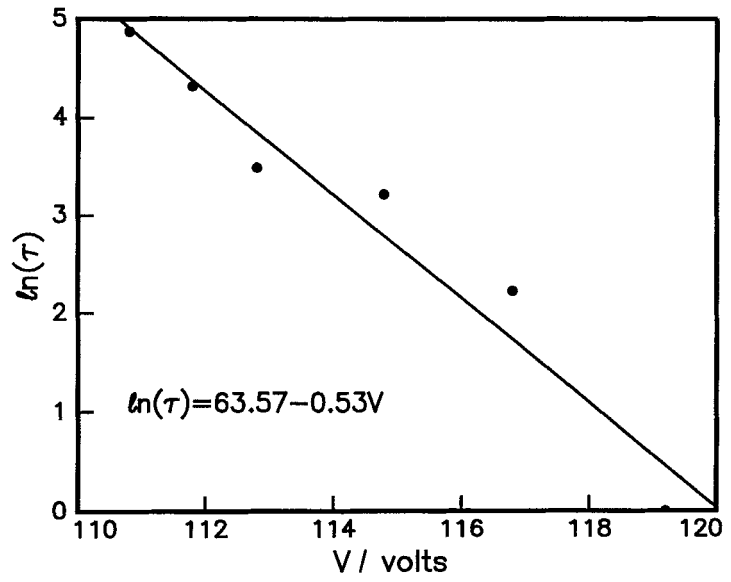

(*a*)

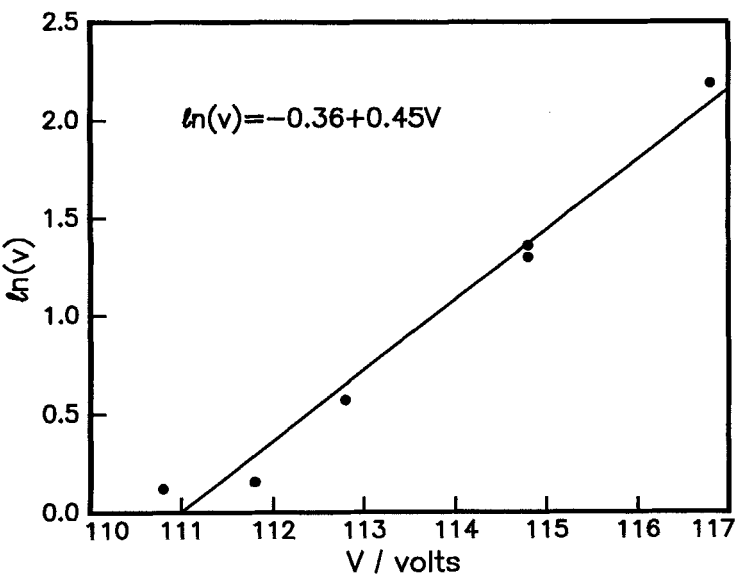

(*b*)

Figure 10. (*a*) The logarithm of the delay time τ is plotted as function of applied voltage. (*b*) The logarithm of the front speed v as a function of applied voltage. From both plots, we obtain for the activation potential Φ: $\Phi \approx 2V$.

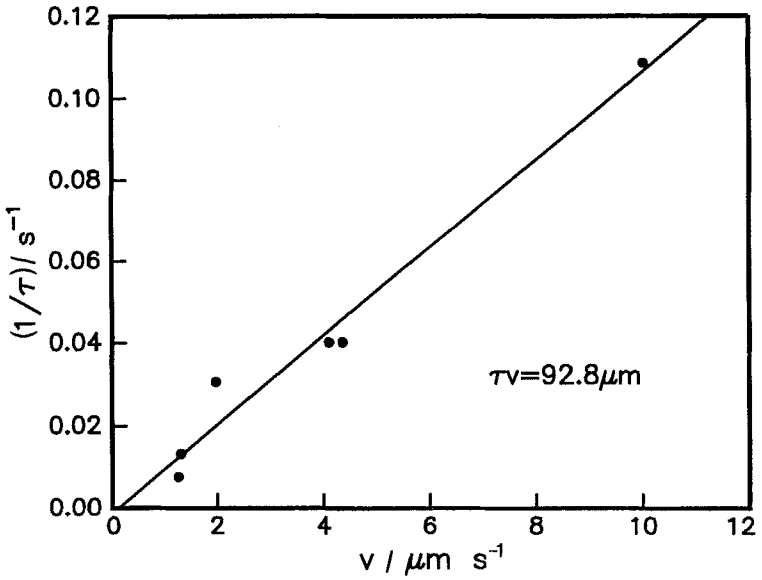

Figure 11. $1/\tau$ is plotted versus the front speed v.

$\Phi \sim 2\,\text{V} \gg 0{\cdot}025\,\text{V}$, i.e. $k_B T$. Indeed, Φ is the same order of magnitude as a cooperative *cis–trans* conformation change such as shown from figure 4 (*a*) to figure 4 (*b*). Because of steric hindrances from neighbouring alkyl chains, this process spreads rapidly within fluid layers as a cooperative effect and propagates slowly perpendicular to the layers giving rise to steps in the space–time plot taken close to 'threshold'.

Figure 11 shows that $1/\tau$ scales with the front speed v such that $L = \tau v \approx 94\,\mu\text{m}$. This scaling is the one expected from a simple time-dependent Ginzburg–Landau equation for front propagation in a purely dissipative system [8]. The length $L = 94\,\mu\text{m}$ obtained is comparable to the grain size from which the data were collected.

A conclusion from these observations (see figures 10 and 11) is that the high frequency field induced transition in a grain (typical dimension $100\,\mu\text{m}$) of a polycrystalline m7tac^{--} sample is imperfect: there is no threshold. Experiments on single crystals of O* are expected to minimize the imperfectness of this transition by eliminating finite size contributions.

Our current picture of this transition is summarized in figure 12. Figure 12 (*a*) is the zero field state, that is identical to the double helix model of Chandani *et al.* [18] for C_{A^*}. Figure 12 (*b*) is the director configuration in a partially unwound state. From the continuous colour changes observed starting at very low voltages, we deduce that the in-plane birefringence is increasing, but the optic axis does not change. We exclude helix unwinding as an option because first, the field of view is perpendicular to the helix axis (no optical rotatory power) and second, the optic axis does not continuously rotate from the low field state to the high field state. The high field state reached in our sample at about 110 V is shown in figure 12 (*c*) with the molecular tilt from both sublattices in the same direction to account for the $\psi \sim 45^\circ$ rotation in the optic axis (see centre of figure 12 (*c*)) shown in figure 7. In the right-hand column of figure 12, we sketch a simple potential description to summarize our observations modelled in the left-hand column. The potential F, with ψ as the order parameter, accounts for the observation of both fast and slow time scales shown in space–time plots (see figure 9) when a field is applied,

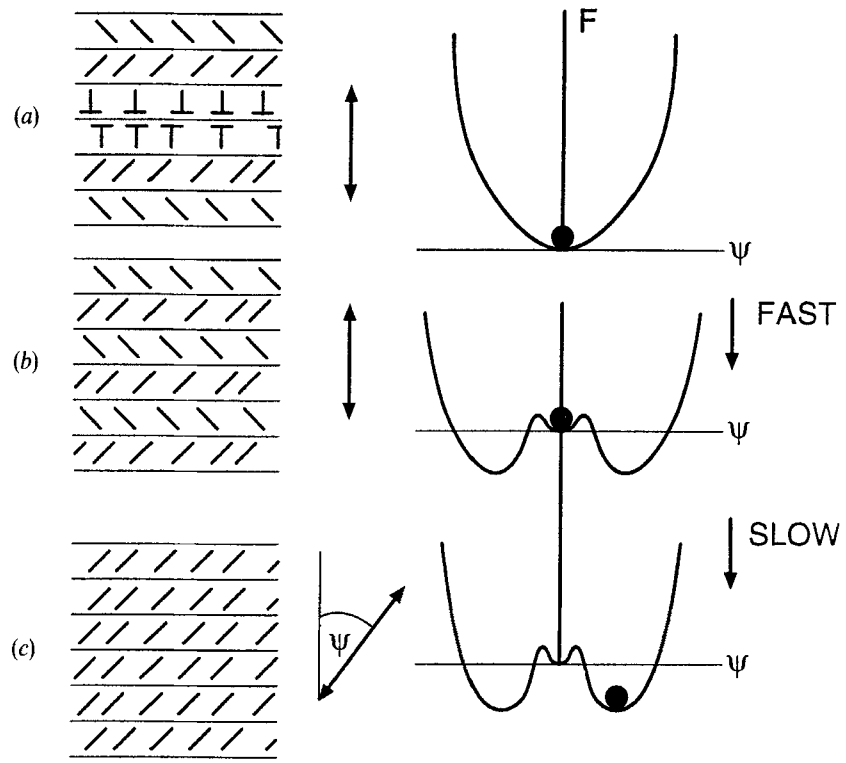

Figure 12. Summary of the response of smectic O* to a large AC field ($E \sim 10\,\mathrm{V}\,\mu\mathrm{m}^{-1}$, $f = 1\,\mathrm{kHz}$). In the figure we display our microscopic picture on the left, the optic axis in the centre and the macroscopic potential F in the right column, where ψ is the order parameter. The solid circle represents the state of the system in the pothetial. (*a*) $E = 0$. (*b*) $E \sim 10\,\mathrm{V}\,\mu\mathrm{m}^{-1}$; metastable state. (*c*) $E \sim 10\,\mathrm{V}\,\mu\mathrm{m}$; stable state reached by front propagation from the metastable state.

i.e. figure 12(*a*)→figure 12(*c*) through the metastable state (see figure 12(*b*)). The potential barrier between the metastable and the stable state represents the energy required to reorient every second layer or, alternatively, a conformational change (as displayed in figure 4), for one of the alkyl chains of m7tac. When the field is turned off, the potential becomes monostable and the system has a single time scale for the spatially homogeneous relaxation to the original helix state. The potential presented underscores the more ordered nature of the high field state (broken continuous rotational symmetry in the plane of the layers, with order parameter ψ) compared to the zero field state with a macroscopic helix structure.

3.4. *Electrooptic effects in smectic O*

In the smectic O phase of m7tac racemate, we observed a linear electrooptic effect shown in the space–time plot in figure 13 taken as 143·3°C, i.e. a temperature greater than the transition temperature to the isotropic liquid of chiral m7tac. This is the most strongly contrasted linear electrooptic effect we observed. Here, a 0·2 Hz square wave of 12 V maximum is applied to the sample. Clearly, figure 13 shows every 2·5 s a change in the optical contrast between crossed polarizers in some but not all regions captured in

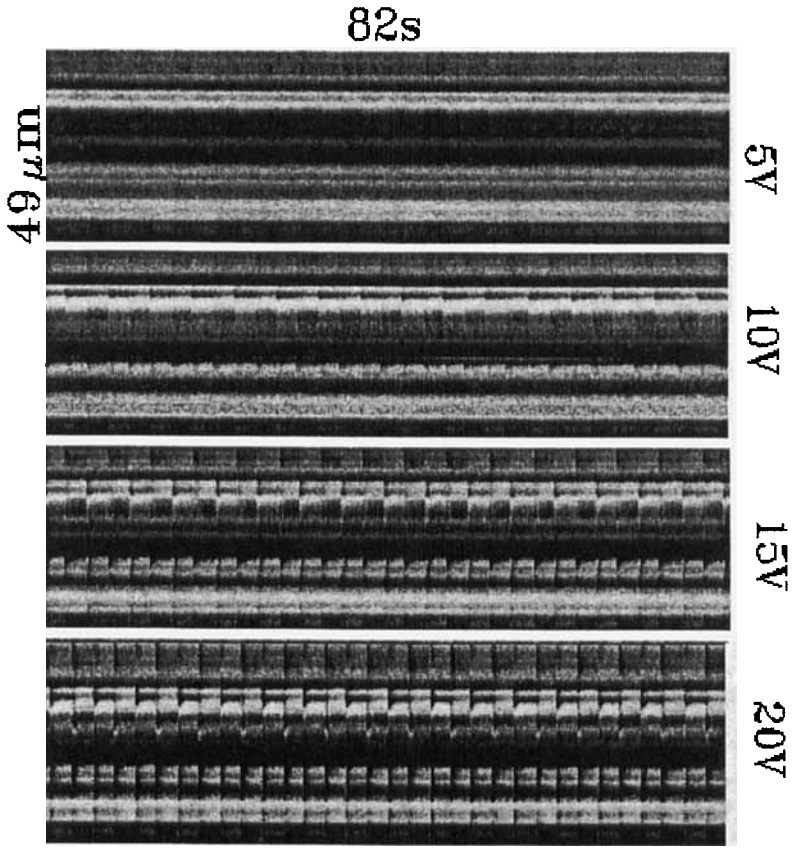

Figure 13. Space–time plot showing linear electrooptic effect in m7tac racemate at 143·3°C.

the space–time plot. At lower temperatures (130°C), the contrast is less good but discernible (see figure 14) when the maximum voltage of the square wave is small.

At higher fields ($\sim 5\,V\,\mu m^{-1}$) and 1 kHz, we observed an electrohydrodynamic (EHD) instability in smectic O (see figure 15). In EHD, the roll pattern is parallel to the layer normal. At larger fields ($\sim V\,\mu m^{-1}$), the pattern coarsened, i.e. its wave number decreased, in time. We did not observe a transition involving a 45° rotation of the optic axis in the racemate up to electric fields of $\sim 10\,V\,\mu m^{-1}$, the field where there was dielectric breakdown of the sample.

In a 1 kHz electric field and between crossed polarizers, we observed objects showing two black brushes that meet at a disclination line (see figure 16) in m7tac racemate. We give our interpretation of this texture at the bottom of figure 16.

In the interpretation at the bottom of figure 16, **c** is the in-plane director. There are two $S = 1/2$ disclinations in **c** (and also **n**) recognized from the two black brushes and two π walls in **c** with colour changes associated with each wall. The walls are more pronounced (i.e. more localized) in the field than they are without the field. Because the two extinction brushes for each $S = 1/2$ disclination are parallel to the crossed polarizers, we deduce that **n**, is parallel to the layer normal as it would be for non-chiral smectic C_M or non-chiral chevron smectics, but not a tilted smectic (see, for example, figure 2). However, in contrast to a C_M phase where the in-plane director **m** is equivalent

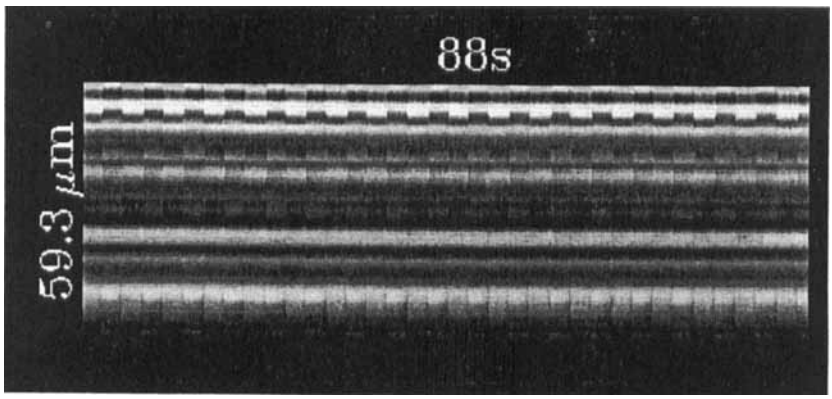

Figure 14. Space–time sequence in m7tac racemate at 130°C for four different voltages.

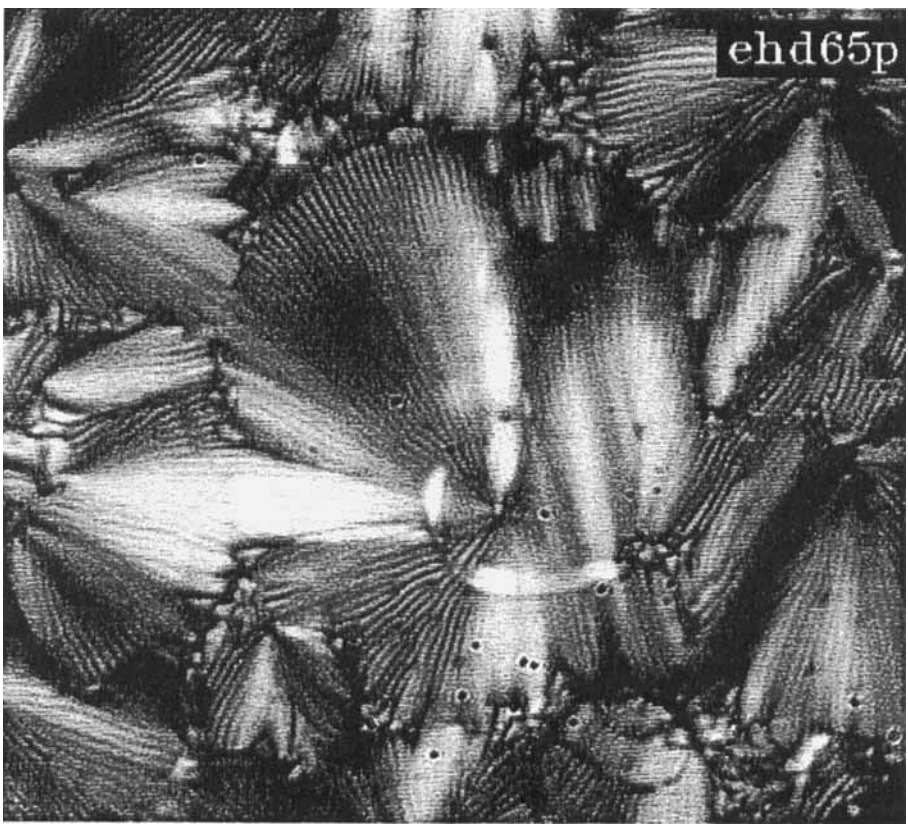

Figure 15. Electrohydrodynamic instability in m7tac racemate at $T = 125°C$, $f = 1$ Hz and $V = 65$ V. The rolls are locally parallel to the layer normal.

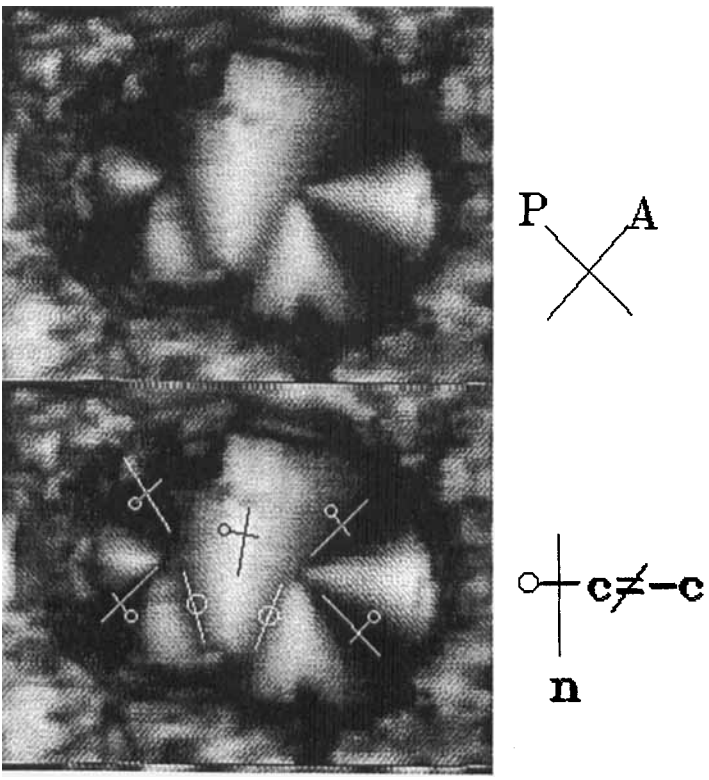

Figure 16. m7tac racemate at 130·4°C in an AC electric field ($f=1$ kHz, $E=11{\cdot}3\,\mathrm{V}\,\mu\mathrm{m}^{-1}$) showing characteristic defects with two dark brushes. The third fainter line is a change in colour.

to $-\mathbf{m}$ and so would not require the π walls, the defect structure shown in figure 16 implies that the in-plane director for smectic O is such that $\mathbf{c}$ is not equivalent to $-\mathbf{c}$.

Thus, the occurrence of π walls in the defect structure shown in figure 16 militates against a tilted smectic or C_M structure for smectic O and is consistent with the symmetry associated with a chevron smectic (see figure 2).

4. Discussion: models for chiral m7tac and its racemate

From figures 5–16, as well as from the electrochromic effect observed in both chiral and racemic m7tac, we deduce the following. First, the observed colour changes in an applied field, are consistent with an electric field enhancement of the in-plane biaxiality of a material with negative dielectric anisotropy. The sign of the in-plane dielectric anisotropy is further supported by the observation of EHD in the racemate (see figure 15). Second, the sharpness of the front (see figure 9) is inconsistent with a continuous unwinding of a helix structure and is associated with an abrupt rotation of the optic axis (see also figure 6).

The question that emerges is: what is the mechanism for the static reorientation of one of the chevron sublattices in a 1 kHz field? It cannot simply be the influence of non-linear electric effects because both figures 12(*b*) and (*c*) are equally compatible for a

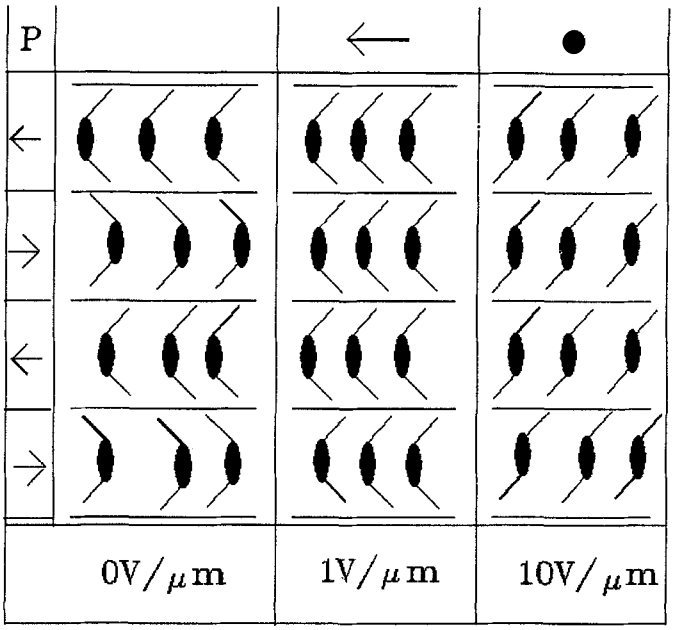

Figure 17. Bilayer antiferroelectric model for chiral m7tac (left hand column) that has a 1 kHz field induced *cis–trans* transformation to a tilted smectic structure (right hand column). The state in the middle shows reorientation of one of the sublattices to form a structure with a field-induced, macroscopic polarization.

material with negative dielectric anisotropy in a large electric field. But, the optical contrast that results from 'freezing in' figure 12 (*b*) is clearly different from a 'frozen' figure 12 (*c*). Why does the system choose figure 12 (*c*)? This question motivated us to consider a new model that is similar in spirit to the chevron models, but with a qualitatively different lamellar structure. Furthermore, it leads to a model that accounts for the enhanced thermal stability of m7tac racemate.

The suggestion is that an electric field induced conformational change is the main mechanism for selection of the structure in the right-hand column of figure 17. Support for this conjecture is the activation potential deduced from the delay time and front speed associated with this transition (see figure 10) that is somewhat smaller but comparable to energies for such transformations in condensed systems.

Suppose m7tac, with two asymmetric carbons (see figure 1) has a ground state conformation for its chiral species, m7tac^{++} and m7tac^{--}, shown in the first column of figure 17 (i.e. two layers of figure 4 (*a*) with opposite polarizations associated with each layer) while m7tac^{+-} and m7tac^{-+} have the conformation shown in figure 4 (*b*) or in the third column of figure 17. As the number of carbons in an alkyl chain determines its orientation relative to the electron-rich aromatic core (see, for example, [14]), the occurrence of smectics O and O* in a homologous series would be sensitive to an 'odd-even' effect [4, 14]. In addition, such a bilayer structure could feasibly mix with the bilayer antiferroelectric compounds [17]. On the other hand, the figure 17 bilayer structure is antiferroelectric, while a ferroelectric *P–E* loop has been observed for m7tac [17]. However, in C_{A*}, the antiferroelectric *P–E* loop is observed at low frequencies and a ferroelectric loop at higher frequencies [19]. With two asymmetric carbons, the

possibility emerges that the observation of an antiferroelectric P–E loop in chiral m7tac may require frequencies even smaller than 1 Hz. Finally, a configuration involving layers of opposing alkyl chains could account for the relative difficulty of drawing freely suspended thick films of chiral m7tac.

On a scale much smaller than the helix pitch, the picture we have in mind is the following. At very low frequencies and small voltages, the 'switching' of each sublattice follows the field so that the average optic axis is normal to the layers. The middle column in figure 17 shows a picture (at an instant in time) for a state with a macroscopic polarization where one of the sublattices is completely switched. With increasing voltage, the probability of *cis–trans* transformation increases. Grain boundaries provide favourable nucleation sites for this transformation in many layers at once, leading to a final state shown in the last column of figure 17.

Models for the racemate must also account for the observation that free standing films of m7tac racemate are weakly biaxial with long lived $S=1$ disclinations and that $S=\pm 1/2$ dispirations are difficult to observe in this geometry. Additional features we keep in mind for the racemate are the relative ease with which we were able to draw freely suspended films and its enhanced thermal stability compared to the chiral species.

The racemate model we propose is similar to existing models [10, 20] but differing in details to include the larger number of m7tac isomers. In figure 18 we suppose that, to optimize a *trans* configuration for the alkyl chains, $m7tac^{++}$ and $m7tac^{--}$ adopt a configuration such as shown for one layer of C_P (see figure 4 (*a*)). In each layer, $m7tac^{++}$ and $m7tac^{--}$ are assumed to be equally mixed. On adjacent layers, we suppose $m7tac^{+-}$ and $m7tac^{-+}$ isomers adopt a configuration more similar to the high field chiral state (see figure 4 (*b*)). Similar to the racemate models for C_A [20] and O [10], the overall structure (see figure 18) is antiferroelectric with C_{2v} symmetry.

This microscopic segregation model lowers the entropy of the racemate compared to a purely chiral species by an amount $\Delta S=6\times 10^{23}\times \ln(2)/650$ giving an excess of latent heat $\Delta L=T\Delta S\approx 0{\cdot}9\,\text{cal g}^{-1}$. This value represents an upper bound for the entropy gain and is comparable, but larger than the observed excess of heat $0{\cdot}7\,\text{cal g}^{-1}$.

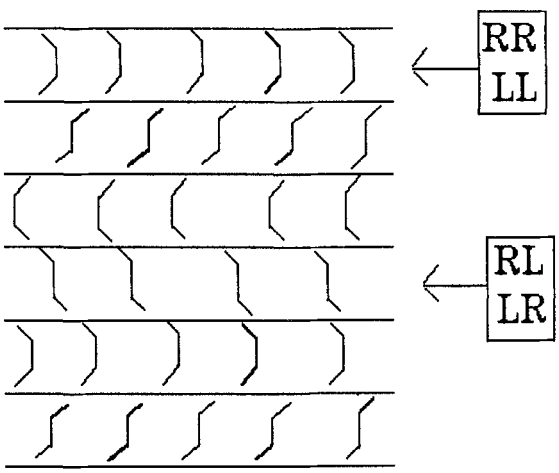

Figure 18. A four layer racemate model based on microsegregation of chiral species.

There are at least two reasons for this reduction: (i) incomplete microsegregation between the species leading to wall energies, and (ii) random stacking of the different types of layers without C_{2v} symmetry.

The weak linear electrooptic effect observed in the racemate in some parts of the sample, but not everywhere, could be attributed to such 'imperfections' in the microsegregation giving rise to macroscopic regimes of predominantly one 'hand' over the other. Such imperfections in segregation also reduce the discrepancy between the estimated and the observed enhancement of the latent heat when wall energies are taken into account.

The overall symmetry of this model is C_{2v} for an 'ideal stacking' (see figure 18) and its polarization state is antiferroelectric. While similar in spirit to existing models [10, 20], this is a four layer model because m7tac has two chiral alkyl chains rather than a single one, so its racemate is composed of four chiral species: (L,L), (R,R), (R,L) and (L,R) and not just two. It is based on our conjecture that smectic O* in chiral m7tac is a double-helixed phase that is locally antiferroelectric (see figure 17). While smectic O* in chiral m7tac has been found to mix with a compound in the C_{A*} phase [17], it is not clear that a four layer structure (see figure 18) will mix with a bilayer structure [10, 20] even though they share the same symmetry, C_{2v}.

In a fluid smectic phase, the in-plane order for figure 18 is biaxial, but weakly so, as the aromatic cores are perpendicular to the layers. In the film geometry, we could expect $S = 1/2$ dispirations in conjunction with a screw dislocation involving two layers rather than just one as in the bilayer chevron model for C_A [12]. As such, a dispiration involving two layers is less likely to form than one involving only a single layer. The biaxiality with **c** not equivalent to $-\mathbf{c}$ in figure 18 is consistent with the formation of long-lived $S = 1$ disclinations.

5. Conclusions and perspectives

Twenty years ago, the known fluid smectic phases were uniaxial smectic A ($D_{\infty h}$) and biaxial smectic C (C_{2h}) phases. Now there are many more. In this paper, we have discussed the more recent new biaxial fluid smectics O, C_A, C_P (C_{2v}) and smectic C_M (D_{2h}). Smectic C_M is unique among the biaxial smectic phases because it is (so far) the only one for which the in-plane director, **m**, is equivalent to $-\mathbf{m}$. Thus, we conclude that smectic C_M is the only biaxial smectic with in-plane fluidity that can exhibit $S = \pm 1/2$ disclinations in **c**. Antiferroelectric chevron smectics (C_A) have the possibility for $S = \pm 1/2$ in-plane disclinations in conjunction with a screw dislocation in the layering [12]. Smectic C phases, ferri- and ferro-electric chevron phases have no possibility to exhibit $S = \pm 1/2$ disclinations in **c**. Chiral smectics with biaxial fluid in-plane order have a helix structure so that the system is globally uniaxial. Consequently, $S = \pm 1/2$ disclinations can occur (and have been observed [11]) when combined with a macroscopic dislocation in the helix pitch—independent of the equivalence of **c** in the plane of a single layer.

We have discussed the different polarization states allowed by the chevron smectics. On the basis of general symmetry arguments, these can range from ferroelectric to antiferroelectric. Indeed, the possibility has been raised for ferroelectricity, ferrielectricity and antiferroelectricity in non-chiral compounds in a chevron structure with polarization vectors in the chevron plane [3].

In chiral compounds, the situation is more complex. Our main conclusion, discussed here, is that the polarization vectors for chiral compounds are locally (i.e. on a scale much smaller than the helix pitch) parallel to the twofold axis in the chevron plane for ferroelectric and ferrielectric states and at some angle to this plane in the antiferroelectric polarization state.

We turn now to specific observations discussed in this paper for m7tac. In general, observations in the high frequency (1 kHz), high field regime are consistent with a negative in-plane dielectric anisotropy. With increasing applied field, the in-plane sample birefringence increased up to about $10\,V\,\mu m^{-1}$ where a transition occurred to another state with optic axis $\sim 45°$ to the low field state. Data from space–time plots of this transition were consistent with an imperfect first order transition with an activation energy of about 2 eV in a domain $\sim 100\,\mu m$. The mechanism for this transition was front propagation of a metastable state into a stable, field induced state.

Motivated by the miscibility results and the sensitivity of smectic O to alkyl chain length [4, 17], we proposed a bilayer chevron structure for the low field state for m7tac. Given the large size of the activation energy associated with the high field state, we attributed the rotation of its optic axis to an electric field induced cooperative conformational change of chiral m7tac to a 'tilted' smectic with the polarization direction perpendicular to its direction before the transition.

Conclusions from this study were incorporated in a four layer 'chevron' model for m7tac racemate that consists of a mixture of equal amounts of $m7tac^{++}$ and $m7tac^{--}$ isomers in a layer and a mixture of equal amounts of $m7tac^{+-}$ and $m7tac^{-+}$ isomers in another layer. This segregation of enantiomers gave an upper bound for the decrease in entropy associated with a racemate compared to a pure chiral species that accounts for the enhanced thermal stability and larger latent heat associated with the racemate transition to the isotropic liquid compared to the chiral compound. We consider the decrease in entropy an upper bound, because, we also observed a weak linear electrooptic effect in the racemate. This suggests that while not changing the estimate for the latent heat excess of the racemate by a large amount, the segregation could be macroscopic rather than microscopic in a less than ideal case. Although the 'ideal' state for this model has the same symmetry (C_{2v}) as the bilayer chevron model [20], it is not clear that a four layer structure will mix with a bilayer one even though they share the same symmetry.

Important open questions include:

(i) What is the role played by grain size on the imperfectness of the transition to the high field state in the chiral compound? Indeed, does it occur in a well-oriented sample and how does it depend on the frequency of the applied field?

(ii) Is the axis associated with the antiferroelectric polarization vector in chiral materials at an angle to the chevron structure as required by general symmetry arguments or perpendicular to it as generally shown in the published [10, 18] models?

(iii) How does the P–E loop for chiral m7tac depend on frequency? What is the P–E loop for the m7tac racemate?

(iv) What is the in-plane order of the high field state? How does the layer spacing depend on the applied field?

It is a pleasure to thank Patrick Keller for the gift of the m7tac compounds. H.R.B. thanks the Deutsche Forschungsgemeinschaft for support of his work. Partial support through NATO CRG-890777 is also acknowledged.

References

[1] LEVELUT, A. M., GERMAIN, C., KELLER, P., LIÉBERT, L., and BILLARD, J., 1983, *J. Phys., Paris*, **44,** 623.

[2] On a microscopic scale (the scale of a smectic layer) starred (*) phases and non-starred phases differ by the absence in the starred phases of a mirror plane. While the notation is not yet universal, on a macroscopic scale, starred phases have a helix structure while unstarred ones do not.

[3] See, for example, BRAND, H. R., CLADIS, P. E., and PLEINER, H., 1992, *Macromolecules*, **25,** 7223.

[4] KELLER, P., 1984, *Molec. Crystals liq. Crystals Lett.*, **102,** 295.

[5] Smectic Q* is reminiscent of blue phases that occur between the isotropic liquid and cholesteric liquid crystals with a tightly twisted pitch (~2000 Å). Apart from the initial observation of Levelut *et al.* of its structure [1], very little is known, even at this time, about smectic Q*. Here we do not discuss our observations made on this phase.

[6] CLADIS, P. E., and BRAND, H. R., 1983 (unpublished).

[7] See, for example, BRAND, H. R., and CLADIS, P. E., 1984, *Molec. Crystals liq. Crystals*, **114,** 207.

[8] CLADIS, P. E., 1991, *J. statist. Phys.*, **62,** 899.

[9] HARDOUIN, F., TINH, N. H., and LEVELUT, A. M., 1982, *J. Phys. Lett.*, **43,** 779.

[10] GALERNE, Y., and LIÉBERT, L., 1990, *Phys. Rev. Lett.*, **64,** 906. GALERNE, Y., and LIÉBERT, L., 1991, *Phys. Rev. Lett.*, **66,** 2891. GALERNE, Y., 1992, *Europhysics Lett.*, **18,** 511.

[11] TAKANISHI, Y., TAKEZOE, H., FUKUDA, A., KOMURA, H., and WATANABE, J., 1992, *J. Mater. Chem.*, **2,** 71.

[12] TAKANISHI, Y., TAKEZOE, H., FUKUDA, A., and WATANABE, J., 1992, *Phys. Rev.* B, **45,** 7684.

[13] MICHELSON, A., CABIB, D., and BENGUIGUI, L., 1977, *J. Phys., Paris*, **38,** 961.

[14] WATANABE, J., and HAYASHI, M., 1988, *Macromolecules*, **21,** 278; 1989, ibid., **22,** 4083.

[15] LEUBE, H., and FINKELMANN, H., 1991, *Makromolek. Chem.*, **192,** 1317.

[16] See, for example, DE GENNES, P. G., 1975, *The Physics of Liquid Crystals* (Clarendon Press).

[17] HEPPKE, G., KLEINEBERG, P., and LÖTZSCH, D., 1992, *21. Freiburger Arbeitstagung Flüssigkristalle* (Freiburg Liquid Crystal Workshop). HEPPKE, G., KLEINEBERG, P., and LÖTZSCH, D., 1993, *Liq. Crystals*, 14 (in the press); the relative magnitudes obtained for the heat of transition of smectics O and O* by these authors agrees with our old results and disagrees with [1]. BÖMELBURG, J., HEPPKE, G., KLEINEBERG, P., LÖTZSCH, D., MERY, S., and SHASHIDHAR, R., 1993, ibid, BÖMELBURG, J. HEPPKE, G., KLEINEBERG, P., LÖTZCH, D., MERY, S., and SHASHIDHAR, R., *Molec. Crystals liq. Crystals Lett.* (in the press).

[18] CHANDANI, A. D. L., HAGIWARA, T., SUZUKI, Y., OUCHI, Y., TAKEZOE, H., and FUKUDA, A., 1988, *Jap. J. appl. Phys.*, **27,** L729. CHANDANI, A. D. L., OUCHI, Y., TAKEZOE, H., FUKUDA, A., TERASHIMA, K., FURUKAWA, K., and KISHI, A., 1989, *Jap. J. appl. Phys.*, **28,** 261. CHANDANI, A. D. L., GORECKA, E., OUCHI, Y., TAKEZOE, H., and FUKUDA, A., 1989, *Jap. J. appl. Phys.*, **28,** 1265. GORECKA, E., CHANDANI, A. D. L., OUCHI, Y., TAKEZOE, H., and FUKUDA, A., 1990, *Jap. J. appl. Phys.*, **29,** 131. HIRAOKA, K., CHANDANI, A. D. L., GORECKA, E., OUCHI, Y., TAKEZOE, H., and FUKUDA, A., 1990, *Jap. J. appl. Phys.*, **29,** 1473. LEE, J., CHANDANI, A. D. L., ITOH, K., OUCHI, Y., TAKEZOE, H., and FUKUDA, A., 1990, *Jap. J. appl. Phys.*, **29,** 1473. LEE, J., CHANDANI, A. D. L., ITOH, K., OUCHI, Y., TAKEZOE, H., and FUKUDA, A., 1990, *Jap. J. appl. Phys.*, **29,** 1122.

[19] See, for example, FUKUI, M., ORIHARA, H., SUZUKI, A., ISHIBASHI, Y., YAMADA, Y., YAMAMOTO, N., MORI, K., NAKAMURA, K., SUZUKI, Y., and KAWAMURA, I., 1990, *Jap. J. appl. Phys.*, **29,** L329. ORIHARA, H., FUJIKAWA, T., ISHIBASHI, Y., YAMADA, Y., YAMAMOTO, N., MORI, K., NAKAMURA, K., SUZUKI, Y., HAGIWARA, T., and KAWAMURA, I., 1990, *Jap. J. appl. Phys.*, **29,** L333. SUZUKI, A., ORIHARA, H., ISHIBASHI, Y., YAMADA, Y., MORI, K., NAKAMURA, K., SUZUKI, Y., HAGIWARA, T., KAWAMURA, I., and FUKUI, M., 1990, *Jap. J. appl. Phys.*, **29,** L336 and references therein.

[20] TAKANISHI, Y., HIRAOKA, K., AGRAWAL, V. K., TAKEZOE, H., FUKUDA, A., and MATSUSHITA, M., 1991, *Jap. J. appl. Phys.*, **30,** 2023.

[21] See, for example, TINKHAM, M., 1964, *Group Theory and Quantum Mechanics* (McGraw-Hill).

[22] MEYER, R. B., LIÉBERT, L., STRZELECKI, L., and KELLER, P., 1975, *J. Phys. Lett., Paris*, **36,** 69. In tilted smectic phases formed by chiral compounds there are no mirror planes leading to a reduction of the symmetry.

[23] See, for example, LE NOBLE, W. J., 1974, *Highlights of Organic Chemistry* (Marcel Dekker Inc.).